Journal of Clinical and Translational Research 2024; 10(2): 165-171

Journal of Clinical and Translational Research

Journal homepage: http://www.jctres.com/en/home

ORIGINAL ARTICLE

Utilizing radiomic features of arterial phase computed tomography for delineating parathyroid adenomas from surrounding anatomical structures

Chime Ezenekwe[1], Michael H. Zhang[2], Irfan Hussain[2], Daniel T. Ginat[3]*

[1]Pritzker School of Medicine, University of Chicago, Chicago, Illinois, United States of America, [2]Department of Radiology, The University of Chicago, Chicago, Illinois, United States of America, [3]School of Medicine, The University of Chicago Medical Center, Chicago, Illinois, United States of America

ARTICLE INFO

Article history:
Received: September 18, 2023
Accepted: November 7, 2023
Published Online: April 25, 2024

Keywords:
Parathyroid adenoma
Radiomics
Texture analysis
Imaging
Four-dimensional computed tomography
Radiology

**Corresponding author:*
Daniel T. Ginat
School of Medicine, The University of Chicago Medical Center, Chicago, Illinois, United States of America.
Email: dtg1@uchicago.edu

ABSTRACT

Aim: The study aimed to correlate radiomic data of four-dimensional computed tomography (4D-CT) with pathology-proven parathyroid adenomas to identify and quantitate select dimensional and textural features that predict parathyroid adenomas with a high degree of confidence, with the ultimate goal of improving the reliability of parathyroid adenoma detection so as to facilitate the subsequent unilateral minimally invasive parathyroidectomy (MIP).

Methods: A total of 144 subjects with a history of neck 4D-CT, parathyroidectomy, and intraoperative pathology-proven parathyroid adenoma(s) were retrospectively reviewed. Following the exclusion of patients with a thyroidectomy, unsuccessful surgery, or indeterminate localization of the parathyroid adenoma on 4D-CT, a preliminary sample of 20 patients was obtained. Four anatomical structures (carotid artery, internal jugular vein, thyroid, and parathyroid adenoma) were segmented twice on 25-second arterial phase axial sections of a 4D-CT, and radiomic data of the shape, first-order, and second-order classes (106 variables) were extracted from the four structures for each patient.

Results: Select radiomic variables among the carotid artery, jugular vein, and thyroid groups exhibited overall significant differences when compared to the parathyroid adenoma data ($P < 0.05$). Further Tukey's *post hoc* analysis revealed that, when the parathyroid adenoma group was treated as the reference, 11/16 shape class, 16/18 first-order class, and 46/69 second-order class variables significantly differ from the carotid artery, jugular vein, and/or thyroid group(s). In addition, we found that the thyroid has distinct textural features compared to the parathyroid group, with 1/18 first-order and 19/69 second-order variables differing significantly between the two ($P < 0.05$). Notably, the texture variables such as dependence non-uniformity, long run emphasis, run percentage, run variance, and busyness exhibited the highest level of differences between the two groups ($P < 0.0001$).

Conclusion: The parathyroid adenoma group is associated with a unique set of radiomic variables in comparison to surrounding anatomy such as the carotid artery, internal jugular vein, and thyroid.

Relevance for Patients: The distinct, quantifiable differences in dimensional and textural features serve as a set of signature markers distinguishing parathyroid adenomas from their surrounding structures in 4D-CT. These attributes obviate the need for invasively locating parathyroid adenomas preoperatively, thereby enhancing the utilization rate of MIP, which has a favorable implication in the overall clinical outcomes.

1. Introduction

Primary hyperparathyroidism (PHPT) is an endocrine disorder characterized by blood serum parathyroid hormone (PTH) levels >8 pmol/L and/or a serum calcium level higher than 2.60 mmol/L [1] caused by one or more of the parathyroid glands secreting an excess amount of PTH. The majority of cases are induced by a single parathyroid adenoma (89%)

DOI: https://doi.org/10.36922/jctr.23.00112

while a small number of cases are caused by multiglandular disease (MGD) (10%), or even more rarely parathyroid carcinoma [2]. PHPT may present asymptomatically or with a myriad of adverse symptoms, classically including renal, cognitive, and/or skeletal abnormalities [3].

Overall, PHPT is the third most common endocrine disorder following diabetes and thyroid disorders [4], thus making it a research area of significant importance, holding promise for improvement of treatment and quality of life. At present, parathyroidectomy is the only curative treatment of PHPT and is recommended in all patients with symptoms [5]. The two common surgical approaches to parathyroidectomy are a bilateral neck exploration (BNE) and a unilateral minimally invasive parathyroidectomy (MIP) [2]. In recent years, the surgical approach has widely changed in favor of MIP as this technique results in reduced surgical times, shorter hospital stays, decreased cost, improved cosmetic appearance, and reduced post-operative fibrosis of the neck, which is beneficial in the case of repeat surgery [1,6]. However, not all patients are candidates for this surgical approach. For example, in the case of MGD when all four glands may be involved, BNE is generally indicated [1]. This procedure involves a surgically intricate and demanding exploration of the delicate neck tissue to examine all four parathyroid glands.

Given the shortcomings and complexities of BNE, MIP is the preferred approach. Proceeding with MIP requires high-level, detailed imaging of the neck anatomy before surgery. At present, sestamibi and/or ultrasound are the most common modalities used for localization [7] but there is no universal protocol for pre-operative imaging. The modality used for imaging is typically based on the surgeon's and radiologist's preferences and knowledge. However, findings from past studies have underscored the importance of using specific imaging modalities according to the actual clinical scenarios. A comprehensive meta-analysis of patients using sestamibi SPECT/CT as a first-line approach for pre-operative imaging has shown a significantly low sensitivity and specificity of 65% and 80%, respectively, when compared to 4D-CT with a sensitivity and specificity of 81% and 89%, respectively [8]. In addition, past studies have shown that 4D-CTs have a concordance rate with intraoperative pathology results of 87%, which surpasses sestamibi and ultrasound with concordance rates of 26.9% and 26.1%, respectively [9]. The high concordance rate of 4D-CTs with intraoperative pathology findings highlights its increasing potential in PHPT detection because inaccurate pre-operative localization necessitates exploration of all parathyroid glands, triggering a shift of surgical approach from MIP to BNE. This data accords with recent studies showing that the mean number of glands explored during parathyroidectomy was significantly lower for patients who received a 4D-CT when compared to patients who were subjected to only nuclear imaging studies [10]. In the past, only difficult cases such as those with negative or discordant ultrasound and sestamibi scans or failed surgery called for the use of 4D-CT scans [11], but with recent findings of the superior efficacy of 4D-CTs, some medical centers have found success transitioning to a new protocol warranting a 4D-CT in replacement of sestamibi in the case of an inconclusive ultrasound finding [10].

There are other factors that might inform a provider's decision on the selection of imaging modality. For example, despite the low costs involved, ultrasounds provide poor imaging results for obese patients and have low sensitivity, and the quality of imaging findings is dependent on the technologist's expertise [11]. Comparatively, 4D-CTs, similarly to sestamibi, expose patients to ionizing radiation, involve higher upfront costs, and require specific radiologist expertise for interpretation.

To avoid the invasive path of BNE surgery, there is growing interest in developing the ability of 4D-CT to identify and localize parathyroid adenomas. By exploring the depth of potential of 4D-CT, it is possible to improve clinical outcomes by providing the necessary accurate pre-operative localization to allow for MIP. Thus, 4D-CT texture analysis has arisen as a particularly promising methodology to non-invasively identify parathyroid adenomas. For this reason, the purpose of this study is to correlate 4D-CT radiomic data to pathology-proven parathyroid adenomas to identify and quantitate select texture features that predict parathyroid adenomas with a high degree of confidence. Ultimately, this study aims to improve the reliability of parathyroid adenoma detection using quantitative CT imaging analysis [2,12].

2. Methods

2.1. Subjects

A total of 144 subjects with a history of a parathyroidectomy procedure for the removal of parathyroid adenoma between 2013 and 2023 were selected for this study through a search of our institution's database using mPower. Patients who received the final pathological diagnosis of parathyroid adenoma, based on intraoperative pathology-proven results of frozen section, were recruited. In addition, only subjects who received a 4D-CT scan of the neck for pre-operative detection and localization of parathyroid adenoma were selected. Patients who had undergone a single parathyroidectomy as well as multiple gland parathyroidectomy were selected. Cases with unsuccessful parathyroidectomy, negative findings, inaccurate localization of parathyroid adenoma on 4D-CT, thyroidectomy before preoperative 4D-CT, or unavailable pathology results were excluded. Fifty eligible cases were identified, of which 20 were randomly selected for inclusion. Figure 1 shows the flow chart of this study featuring the inclusion criteria. This study was approved by the institutional review board at the University of Chicago.

2.2. Image analysis

The 25-second arterial phase of each patient's 4D-CT neck scan (kVp: 120; mAs: 200; slice thickness: 3 mm) was used for analysis. Three anatomical structures (carotid artery, jugular vein, and thyroid gland) were chosen to differentiate from the parathyroid adenoma. An axial section of the 25-second arterial phases containing the largest area of each of the four structures was selected. Segmentation of the carotid artery, jugular vein, thyroid, and parathyroid adenoma was completed on the selected axial series of each patient using the 3D Slicer image computing platform. Figure 2 displays a representative resultant image

DOI: https://doi.org/10.36922/jctr.23.00112

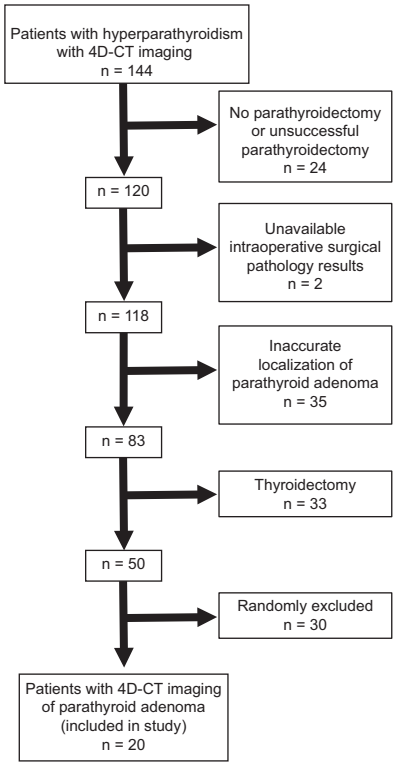

Figure 1. Flow chart of the present study and inclusion criteria.

after the segmentation technique was employed. The radiomic data were extracted and collected from the four structures of interest for each patient to be analyzed. Segmentation of a second axial section, from the same 25-second arterial phase scan, was completed for the carotid, jugular, and thyroid for the purpose of comparing the texture features to the previous segmentation to ensure consistency for each structure. The average of these two data points was taken for final analyses to ensure that the radiomic data are uniform between the two selected axial sections for each subject, reducing the possibility of artifacts or abnormalities impacting radiomic data.

2.3. Data analysis

Radiomic variables of the shape, first-order, and second-order classes were extracted from the segmentations of each of the 20 patients. In a categorical sense, data from the carotid artery, jugular vein, thyroid, and parathyroid adenoma were referred to as four distinct groups: carotid, jugular, thyroid, and parathyroid groups, respectively. Analysis of variance (ANOVA) was conducted to assess if there are statistical differences between the carotid, jugular, and thyroid groups when compared to the reference group, *i.e.*, parathyroid group. Subsequently, Tukey's HSD *post hoc* test was performed to compare differences in radiomic variables between specific anatomical structure groups. Variables that differ significantly between the parathyroid group and the other three groups were noted as radiomic variables that could potentially be used to differentiate the structures.

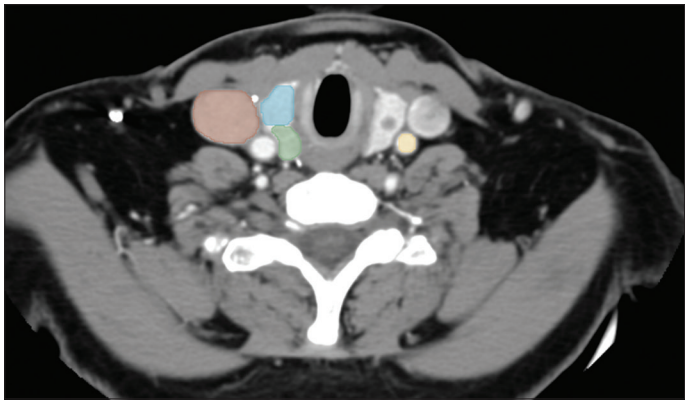

Figure 2. A representative resultant image following segmentation. Notes: Red represents jugular vein, yellow represents carotid artery, green represents parathyroid adenoma, and blue represents thyroid.

3. Results

A total of 144 patients were identified from the University of Chicago patient database for this study of which 20 were selected based on the exclusion criteria detailed in Figure 1. Patients who had undergone 4D-CT localization studies conducted between 2013 and 2023 were selected. The ages of the cohort analyzed ranged from 23 to 77 years with an average of 56.7 years. Patients of a range of races were analyzed, including White (40%), Black/African American (55%), and Asian/Mideast Indian (5%). The location of the parathyroid adenoma of interest for all patients falls into one of two categories: thyroid adjacent (85%) or ectopic/mediastinum (17.6%). Thyroid adjacent refers to any area adjacent to the thyroid gland, while ectopic/mediastinum is defined as any area not adjacent to the thyroid gland. Further details on cohort demographics can be found in Table 1.

Results of an ANOVA analysis revealed overall significant differences in select radiomic variables among the carotid artery, jugular vein, and thyroid groups when compared to the reference group, parathyroid adenoma data ($P < 0.05$). Upon completion of a follow-up Tukey's HSD *post hoc* test to compare specific groups, using the parathyroid group as the reference, we found that 11/16 shape class, 16/18 first-order class, and 46/69 second-order class variables significantly differ from the carotid artery, jugular vein, and/or thyroid group(s).

When comparing the thyroid to the parathyroid group, we found that the thyroid has distinct textural features, with 1/18 first-order and 19/69 second-order variables differing significantly between the two groups ($P < 0.05$). Notably, the texture variables such as dependence non-uniformity, long run emphasis, run percentage, run variance, and busyness exhibited the highest level of differences between the two groups ($P < 0.0001$). An isolated comparison revealed more subtle textural differences between the carotid artery group and the parathyroid group. We found that 14/18 first-order and 27/69 second-order variables presented significant differences between the two groups ($P < 0.05$), of which 12 variables were significant at the level of $P < 0.0001$. In our analysis of the internal jugular vein compared to

DOI: https://doi.org/10.36922/jctr.23.00112

the parathyroid group, we found that there were minimal textural distinctions between the two groups. We observed 5/18 first-order and 12/69 second-order variables differing significantly between the two ($P < 0.05$), of which only 2 variables were significant at the level of $P < 0.0001$. All significant variables and their respective level of significance can be found in Tables 2-4 for each anatomical group.

Table 1. Demographic information

Characteristics	N	%	Average
Age	20	-	56.71
Sex			
Male	8	40	-
Female	12	60	-
Race			
White	8	40	-
Black/African American	11	55	-
Asian/Mideast Indian	1	5	-
Hispanic/Latinx	0	0	-
Nodule location			
Ectopic/mediastinum	3	15	-
Thyroid adjacent	17	85	-

4. Discussion

The carotid artery and jugular vein are obvious anatomical landmarks and easily discernable from lesions for radiologists on 4D-CTs but not necessarily for computers. The long-term goal from this study is computer automated, texturally informed prediction and localization of parathyroid adenomas. With this in mind, radiomic data from the carotid artery and jugular vein, often in close proximity to parathyroid lesion and also hyperattenuating on post-contrast CT, is required to add to a model's inventory of patterns for predicting and differentiating lesions from surrounding anatomy with increased confidence.

Table 2. Predictive variables of significance for thyroid group

Variable	Variable class	Estimated difference in means	95% CI lower limit	95% CI upper limit	P_{adj}	Significance
Id	gclm	−1.83E-01	−2.96E-01	−7.02E-02	3.29E-04	**
Idm	gclm	−4.37E+00	−7.15E+00	−1.59E+00	5.28E-04	*
Idn	gclm	−5.45E+00	−7.64E+00	−3.27E+00	3.47E-08	**
InverseVariance	gclm	−4.04E+00	−6.51E+00	−1.57E+00	2.95E-04	**
DependenceNonUniformity	gclm	−4.55E+00	−7.24E+00	−1.85E+00	1.79E-04	****
GrayLevelNonUniformity	gclm	−4.40E+00	−7.05E+00	−1.75E+00	2.32E-04	***
SmallDependenceLowGrayLevelEmphasis	gclm	−2.12E+02	−3.22E+02	−1.01E+02	1.82E-05	**
LongRunEmphasis	gclm	−5.37E+00	−7.32E+00	−3.41E+00	1.92E-09	****
RunEntropy	gclm	−1.86E+02	−2.79E+02	−9.38E+01	6.76E-06	***
RunLengthNonUniformityNormalized	gclm	−2.16E+02	−3.29E+02	−1.03E+02	2.05E-05	***
RunPercentage	gclm	−6.04E+01	−1.20E+02	−7.89E-01	4.59E-02	****
RunVariance	gclm	−2.38E+07	−4.21E+07	−5.54E+06	5.42E-03	****
ShortRunEmphasis	gclm	−7.63E+01	−1.48E+02	−4.77E+00	3.20E-02	**
LargeAreaEmphasis	gclm	−6.47E+01	−1.29E+02	−3.60E-02	4.98E-02	*
LargeAreaLowGrayLevelEmphasis	gclm	−1.14E+07	−1.90E+07	−3.78E+06	1.05E-03	***
ZonePercentage	gclm	−6.56E-03	−1.18E-02	−1.34E-03	7.91E-03	*
ZoneVariance	gclm	−4.72E+01	−7.20E+01	−2.23E+01	2.19E-05	*
Busyness	gclm	−1.31E+02	−2.38E+02	−2.43E+01	9.84E-03	****
Coarseness	gclm	1.31E-02	4.04E-03	2.22E-02	1.65E-03	**
TotalEnergy	First order	−1.93E+02	−3.29E+02	−5.60E+01	2.23E-03	*
MajorAxisLength	shape	−6.67E-01	−9.75E-01	−3.59E-01	1.38E-06	****
Maximum2DDiameterColumn	shape	8.73E-02	8.15E-03	1.66E-01	2.48E-02	****
Maximum2DDiameterRow	shape	5.01E-02	1.36E-02	8.66E-02	3.03E-03	****
Maximum2DDiameterSlice	shape	−4.48E+00	−7.53E+00	−1.42E+00	1.37E-03	****
Maximum3DDiameter	shape	−9.51E-02	−1.77E-01	−1.34E-02	1.60E-02	****
MeshVolume	shape	−7.79E-01	−1.29E+00	−2.67E-01	8.38E-04	****
MinorAxisLength	shape	1.04E-01	2.61E-02	1.81E-01	4.12E-03	****
Sphericity	shape	−1.83E-01	−2.96E-01	−7.02E-02	3.29E-04	*
SurfaceArea	shape	−4.37E+00	−7.15E+00	−1.59E+00	5.28E-04	****
VoxelVolume	shape	−5.45E+00	−7.64E+00	−3.27E+00	3.47E-08	****

Notes: (i) Parathyroid group is the reference group for all comparisons in the table.
(ii) Positive values indicate that the mean of the parathyroid group is lower and *vice versa*.
(iii) ns: Not significant; *0.01< P < 0.05; ** 0.001< P < 0.01; *** 0.0001< P < 0.001; **** P<0.0001.

DOI: https://doi.org/10.36922/jctr.23.00112

Table 3. Predictive variables of significance for carotid group

Variable	Variable class	Estimated difference in means	95% CI lower limit	95% CI upper limit	P_{adj}	Significance
Elongation	shape	−2.93E-01	−4.06E-01	−1.80E-01	1.09E-08	****
MajorAxisLength	shape	3.16E+00	3.84E-01	5.95E+00	1.93E-02	*
Maximum2DDiameterSlice	shape	3.12E+00	4.22E-01	5.81E+00	1.68E-02	*
Maximum3DDiameter	shape	3.04E+00	3.94E-01	5.69E+00	1.79E-02	*
Sphericity	shape	−8.87E-02	−1.69E-01	−8.84E-03	2.35E-02	*
Percentile10	First order	−1.32E+02	−1.92E+02	−7.23E+01	8.13E-07	****
Percentile90	First order	−1.64E+02	−2.33E+02	−9.56E+01	1.17E-07	****
Entropy	First order	−3.87E-01	−7.71E-01	−2.90E-03	4.76E-02	*
InterquartileRange	First order	−1.64E+01	−3.06E+01	−2.26E+00	1.65E-02	*
Maximum	First order	−1.57E+02	−2.29E+02	−8.59E+01	9.24E-07	****
MeanAbsoluteDeviation	First order	−1.14E+01	−2.00E+01	−2.77E+00	4.70E-03	**
Mean	First order	−1.57E+02	−2.21E+02	−9.19E+01	8.14E-08	****
Median	First order	−1.68E+02	−2.35E+02	−1.00E+02	3.80E-08	****
Minimum	First order	−1.05E+02	−1.60E+02	−4.95E+01	2.19E-05	****
Range	First order	−5.29E+01	−1.03E+02	−2.97E+00	3.36E-02	*
RobustMeanAbsoluteDeviation	First order	−7.79E+00	−1.39E+01	−1.73E+00	6.21E-03	**
RootMeanSquared	First order	−1.56E+02	−2.21E+02	−9.18E+01	8.15E-08	****
Skewness	First order	6.40E-01	1.52E-01	1.13E+00	5.12E-03	**
Variance	First order	−1.21E+03	−2.25E+03	−1.75E+02	1.55E-02	*
Autocorrelation	gclm	−2.77E+01	−4.78E+01	−7.70E+00	2.77E-03	**
ClusterShade	gclm	4.17E+01	9.74E-01	8.24E+01	4.27E-02	*
ClusterTendency	gclm	−5.04E+00	−9.90E+00	−1.89E-01	3.86E-02	*
Contrast	gclm	−1.01E+00	−1.71E+00	−3.11E-01	1.64E-03	**
DifferenceAverage	gclm	−2.87E-01	−4.67E-01	−1.08E-01	4.02E-04	***
DifferenceEntropy	gclm	−4.52E-01	−6.71E-01	−2.34E-01	3.83E-06	****
DifferenceVariance	gclm	−5.71E-01	−9.44E-01	−1.98E-01	7.76E-04	***
Id	gclm	6.89E-02	1.77E-02	1.20E-01	3.79E-03	**
Idm	gclm	−2.93E-01	−4.06E-01	−1.80E-01	1.09E-08	**
JointAverage	gclm	3.16E+00	3.84E-01	5.95E+00	1.93E-02	***
SumAverage	gclm	3.12E+00	4.22E-01	5.81E+00	1.68E-02	***
SumSquares	gclm	3.04E+00	3.94E-01	5.69E+00	1.79E-02	*
GrayLevelVariance	gclm	−8.87E-02	−1.69E-01	−8.84E-03	2.35E-02	*
HighGrayLevelEmphasis	gclm	−1.32E+02	−1.92E+02	−7.23E+01	8.13E-07	**
SmallDependenceEmphasis	gclm	−1.64E+02	−2.33E+02	−9.56E+01	1.17E-07	****
HighGrayLevelRunEmphasis	gclm	−3.87E-01	−7.71E-01	−2.90E-03	4.76E-02	*
RunLengthNonUniformityNormalized	gclm	−1.64E+01	−3.06E+01	−2.26E+00	1.65E-02	**
ShortRunEmphasis	gclm	−1.57E+02	−2.29E+02	−8.59E+01	9.24E-07	***
ShortRunHighGrayLevelEmphasis	gclm	−1.14E+01	−2.00E+01	−2.77E+00	4.70E-03	**
SizeZoneNonUniformity	gclm	−1.57E+02	−2.21E+02	−9.19E+01	8.14E-08	***
SizeZoneNonUniformityNormalized	gclm	−1.68E+02	−2.35E+02	−1.00E+02	3.80E-08	****
SmallAreaEmphasis	gclm	−1.05E+02	−1.60E+02	−4.95E+01	2.19E-05	****
ZonePercentage	gclm	−5.29E+01	−1.03E+02	−2.97E+00	3.36E-02	****
Complexity	gclm	−7.79E+00	−1.39E+01	−1.73E+00	6.21E-03	*
Strength	gclm	−1.56E+02	−2.21E+02	−9.18E+01	8.15E-08	**
SmallDependenceHighGrayLevelEmphasis	gclm	6.40E-01	1.52E-01	1.13E+00	5.12E-03	**
GrayLevelNonUniformityNormalized	gclm	−1.21E+03	−2.25E+03	−1.75E+02	1.55E-02	*

Notes: (i) Parathyroid group is the reference group for all comparisons in the table.
(ii) Positive values indicate that the mean of the parathyroid group is lower and *vice versa*.
(iii) ns: Not significant; *0.01< P < 0.05; ** 0.001< P < 0.01; *** 0.0001< P < 0.001; ****P<0.0001.

DOI: https://doi.org/10.36922/jctr.23.00112

In addition, parathyroid lesions are most often located directly adjacent to the thyroid, making it difficult for radiologists and computers alike to distinguish between the two with a high level of confidence. Thus, our selection and comparison of the thyroid to parathyroid lesions in this study are particularly important. Our data suggest that parathyroid lesions are associated with a unique set of radiomic variables when compared to the thyroid. These distinct, quantifiable differences revealed will be of use in creating a texture signature specific to parathyroid adenomas. This signature could utilize dimensional and textural differences between the parathyroid adenoma and surrounding anatomy to create models that predict potential lesions and more precisely localize parathyroid adenomas.

Naturally, the next step in our application of this data is to investigate the performance of a parathyroid adenoma texture signature in models differentiating lesions from surrounding neck anatomy on 4D-CTs. For example, a recent study has had moderate success using imaging characteristics of parathyroid adenomas to predict the pathology of anterior mediastinal masses [13]. Another study achieved notable results by applying radiomic data extracted from parathyroid scintigraphy to algorithms to compare the utility and performance of different models [14]. Considering the recent success of other applications of radiomic data in the field, findings of this study are anticipated to make a meaningful contribution to future advances in parathyroid adenoma identification and localization. Ultimately, the ability to non-invasively localize parathyroid adenomas preoperatively could in turn translate to broader utilization of MIP, resulting in overall improved clinical outcomes [1,2].

Several limitations of this study should be acknowledged. The most prominent shortcoming of this study is that the relatively small sample size was n=20. In addition, the retrospective nature of the study and selection bias might influence the generalizability of the results. Further investigation is needed to validate our findings and warrant application in a clinical setting.

5. Conclusion

Our observations grounded in the statistical significance of several radiomic variables within the shape, first-order, and second-order feature classes in differentiating parathyroid adenoma from surrounding neck anatomy, such as carotid artery,

Table 4. Predictive variables of significance for jugular group

Variable	Variable class	Estimated difference in means	95% CI lower limit	95% CI upper limit	P_{adj}	Significance
Elongation	shape	−1.83E−01	−2.96E−01	−7.02E−02	3.29E−04	***
MajorAxisLength	shape	−4.37E+00	−7.15E+00	−1.59E+00	5.28E−04	***
Maximum2DDiameterColumn	shape	−5.45E+00	−7.64E+00	−3.27E+00	3.47E−08	****
Maximum2DDiameterRow	shape	−4.04E+00	−6.51E+00	−1.57E+00	2.95E−04	***
Maximum2DDiameterSlice	shape	−4.55E+00	−7.24E+00	−1.85E+00	1.79E−04	***
Maximum3DDiameter	shape	−4.40E+00	−7.05E+00	−1.75E+00	2.32E−04	***
MeshVolume	shape	−2.12E+02	−3.22E+02	−1.01E+02	1.82E−05	****
MinorAxisLength	shape	−5.37E+00	−7.32E+00	−3.41E+00	1.92E−09	****
SurfaceArea	shape	−1.86E+02	−2.79E+02	−9.38E+01	6.76E−06	****
VoxelVolume	shape	−2.16E+02	−3.29E+02	−1.03E+02	2.05E−05	****
Percentile10	First order	−6.04E+01	−1.20E+02	−7.89E−01	4.59E−02	*
Energy	First order	−2.38E+07	−4.21E+07	−5.54E+06	5.42E−03	**
Maximum	First order	−7.63E+01	−1.48E+02	−4.77E+00	3.20E−02	*
Mean	First order	−6.47E+01	−1.29E+02	−3.60E−02	4.98E−02	*
TotalEnergy	First order	−1.14E+07	−1.90E+07	−3.78E+06	1.05E−03	**
Idmn	gclm	−6.56E−03	−1.18E−02	−1.34E−03	7.91E−03	**
DependenceNonUniformity	gclm	−4.72E+01	−7.20E+01	−2.23E+01	2.19E−05	****
GrayLevelNonUniformity	gclm	−1.31E+02	−2.38E+02	−2.43E+01	9.84E−03	**
SmallDependenceLowGrayLevelEmphasis	gclm	1.31E−02	4.04E−03	2.22E−02	1.65E−03	**
LongRunHighGrayLevelEmphasis	gclm	−1.93E+02	−3.29E+02	−5.60E+01	2.23E−03	**
RunEntropy	gclm	−6.67E−01	−9.75E−01	−3.59E−01	1.38E−06	****
RunPercentage	gclm	8.73E−02	8.15E−03	1.66E−01	2.48E−02	*
ShortRunLowGrayLevelEmphasis	gclm	5.01E−02	1.36E−02	8.66E−02	3.03E−03	**
SizeZoneNonUniformity	gclm	−4.48E+00	−7.53E+00	−1.42E+00	1.37E−03	**
SmallAreaEmphasis	gclm	−9.51E−02	−1.77E−01	−1.34E−02	1.60E−02	*
ZoneEntropy	gclm	−7.79E−01	−1.29E+00	−2.67E−01	8.38E−04	***
Coarseness	gclm	1.04E−01	2.61E−02	1.81E−01	4.12E−03	**

Notes: (i) Parathyroid group is the reference group for all comparisons in the table.
(ii) Positive values indicate that the mean of the parathyroid group is lower and *vice versa*.
(iii) ns: Not significant; *$0.01<P<0.05$; **$0.001<P<0.01$; ***$0.0001<P<0.001$; ****$P<0.0001$.

DOI: https://doi.org/10.36922/jctr.23.00112

jugular vein, and thyroid, underline the projected utility of radiomic data in clinical localization of parathyroid adenomas. Used in conjunction with conventional indicators, radiomic data could prove to be a powerful tool in pre-operative localization of lesions, given that this line of questioning is further pursued with larger sample sizes and controlled research models.

Acknowledgments

None.

Funding

This research was supported in part by the Burroughs Welcome Fund Early Scientific Training Program to Prepare for Research Excellence Post-Graduation (BEST-PREP).

Conflict of Interest

The authors declare no conflicts of interest.

Ethics Approval and Consent to Participate

This work has been approved by the IRB. The IRB ID is IRB14-0749.

Consent for Publication

Consent was obtained through IRB.

Availability of Data

Data are available from the corresponding author upon reasonable request.

References

[1] Van Dalen A, Smit CP, Van Vroonhoven TJ, Burger H, De Lange EE. Minimally Invasive Surgery for Solitary Parathyroid Adenomas in Patients with Primary Hyperparathyroidism: Role of US with Supplemental CT. Radiology 2001;220:631-9.
doi: 10.1148/radiol.2203000998

[2] Johnson NA, Tublin ME, Ogilvie JB. Parathyroid Imaging: Technique and Role in the Preoperative Evaluation of Primary Hyperparathyroidism. AJR Am J Roentgenol 2007;188:1706-15.
doi: 10.2214/AJR.06.0938

[3] Bilezikian JP, Cusano NE, Khan AA, Liu JM, Marcocci C, Bandeira F. Primary Hyperparathyroidism. Nat Rev Dis Primer 2016;2:16033.
doi: 10.1038/nrdp.2016.33

[4] Kelly HR, Bunch PM. Parathyroid Computed Tomography: Pearls, Pitfalls, and Our Approach. Neuroimaging Clin N Am 2022;32:413-31.
doi: 10.1016/j.nic.2022.01.006

[5] Walker MD, Silverberg SJ. Primary hyperparathyroidism. Nat Rev Endocrinol 2018;14:115-25.
doi: 10.1038/nrendo.2017.104

[6] Walsh NJ, Sullivan BT, Duke WS, Terris DJ. Routine Bilateral Neck Exploration and Four-Gland Dissection Remains Unnecessary in Modern Parathyroid Surgery. Laryngoscope Investig Otolaryngol 2019;4:188-92.
doi: 10.1002/lio2.223

[7] Kuo LE, Bird SH, Lubitz CC, Pandian TK, Parangi S, Stephen AE. Four-Dimensional Computed Tomography (4D-CT) for Preoperative Parathyroid Localization: A Good Study but are we Using it? Am J Surg 2022;223:694-8.
doi: 10.1016/j.amjsurg.2021.09.015

[8] Strauss SB, Shatzkes DR. Beyond the AJR: Largest Systematic Review to Date Confirms High Accuracy of 4D CT in Parathyroid Localization. Am J Roentgenol 2023;220:305-5.
doi: 10.2214/AJR.22.28127

[9] Cruz-Centeno N, Longoria-Dubocq T, Mendez-Latalladi W. Efficacy of 4D CT Scan in Re-Operative Parathyroid Surgery. Am Surg 2022;88:1549-50.
doi: 10.1177/00031348221083938

[10] Jategaonkar AA, Lerner DK, Cooke P, Kirke D, Genden EM, Trosman SJ. Implementation of a 4-Dimensional Computed Tomography Protocol for Parathyroid Adenoma Localization. Am J Otolaryngol 2021;42:102907.
doi: 10.1016/j.amjoto.2021.102907

[11] Itani M, Middleton WD. Parathyroid Imaging. Radiol Clin North Am 2020;58:1071-83.
doi: 10.1016/j.rcl.2020.07.006

[12] Perrier ND, Edeiken B, Nunez R, Gayed I, Jimenez C, Busaidy N, *et al*. A Novel Nomenclature to Classify Parathyroid Adenomas. World J Surg 2009;33:412-6.
doi: 10.1007/s00268-008-9894-0

[13] Mayoral M, Pagano AM, Araujo-Filho JA, Zheng J, Perez-Johnston R, Tan KS, *et al*. Conventional and Radiomic Features to Predict Pathology in the Preoperative Assessment of Anterior Mediastinal Masses. Lung Cancer 2023;178:206-12.
doi: 10.1016/j.lungcan.2023.02.014

[14] Valavi S, Hajianfar G, Masoudi SF, Maghsudi M, Sohrabi M, Rajabi AB, *et al*. Parathyroid Adenoma Subtype Decoding by Using SPECT Radiomic Features and Machine Learning Algorithms. J Nucl Med 2022;63:3235.